ELSEVIER

Biophysical Chemistry 124 (2006) 73–79

Biophysical Chemistry

http://www.elsevier.com/locate/biophyschem

Structural characterization of the 5′ untranslated RNA of hepatitis C virus by vibrational spectroscopy

Arantxa Rodríguez-Casado [a], Javier Bartolomé [b], Vicente Carreño [b], Marina Molina [c], Pedro Carmona [a,*]

[a] *Instituto de Estructura de la Materia (CSIC), Serrano 121, 28006 Madrid, Spain*
[b] *Fundación para el Estudio de las Hepatitis Virales (FEHV), Madrid, Spain*
[c] *Departamento de Química Orgánica I, Escuela Universitaria de Optica, Universidad Complutense, 28037 Madrid, Spain*

Received 29 March 2006; received in revised form 19 June 2006; accepted 20 June 2006
Available online 7 July 2006

Abstract

Raman and FTIR spectroscopy have been used to characterize the structure of 5′untranslated region (5′UTR, 342-mer RNA) of the HCV genome. The study of the 750–850 cm^{-1} Raman spectral domain of the ribose-phosphate backbone reveals that the percentage of nucleobases involved in double helix–loop junctions is 19±1%, which is very close to that of a theoretical secondary structure model (18.7%) proposed on the basis of comparative sequence analysis and thermodynamic modelling. In addition, about 68±2% of the bases are helically ordered having *C(3′)-endo* ribofuranose pucker. FTIR-monitored H/D exchange provides the following results: (a) base-paired guanine and cytosine nucleobases show the lowest rate of isotopic exchange, and some synchronous intensity changes of marker bands of A·U pair and single stranded adenine are consistent with the presence of A*A·U triplets; (b) the vibrational coupling between the ribose ether C–O stretching and 2′OH bending motions reveals that helical regions of 5′UTR RNA are characterized by hydrogen bonding between the 2′OH ribose groups and the ether oxygen atoms of neighbouring ribose residues.

Keywords: 5′UTR RNA structure; Raman spectroscopy; Infrared spectroscopy; HCV virus

1. Introduction

Hepatitis C virus (HCV) is an enveloped positive-stranded RNA virus that has been identified as the agent responsible for the majority of cases of non-A, non-B hepatitis. In about 85% of cases, infection becomes chronic, persisting for an indefinite length of time, often leading to liver cirrhosis and hepatocellular carcinoma [1]. More than 100 strains of HCV have been identified till date, which are grouped into six major genotypes [2]. Comparison of the 5′untranslated region (5′UTR) among the six genotypes shows that this region is highly conserved with a sequence homology of around 92–98% [3], whereby the structural study of this viral RNA region is of interest.

In order to develop drugs against HCV, structure based design is crucial. For instance, bulged RNA is known to be more susceptible to cleavage than RNA in a helical structure and is therefore particularly interesting as a target for artificial nucleases [4–6]. In this connection, it has been suggested that the sugar conformations at the cleavage sites have a major impact on the rate of cleavage [5,6]. Therefore, it would be also of value to have access to a method that gives an estimate of sugar conformations in RNA without carrying out an extensive structural study. X-ray crystallography could be considered in the determination of viral RNA architecture, but up to date only some relatively short fragments of the 5′UTR region from HCV RNA have yielded crystals that are suitable for diffraction analysis [7]. Infrared and Raman spectroscopies can provide answer to this question because of the developments in their methods achieved during the last decade. Moreover, the infrared and Raman marker bands occurring at different frequency regions provide an instant snapshot of other features of nucleic acid structure, giving information on base pairing/base stacking and nature of helix [8,9].

* Corresponding author. Tel.: +34 91 5616800; fax: +34 91 5645557.
E-mail address: p.carmona@iem.cfmac.csic.es (P. Carmona).

0301-4622/$ - see front matter © 2006 Elsevier B.V. All rights reserved.
doi:10.1016/j.bpc.2006.06.010

To deconvolute highly overlapped infrared and Raman bands belonging to the same type of structural details, hydrogen–deuterium (H/D) exchange is also useful. Since the protons of each conformation do not exchange simultaneously, the contributions from different structures to the overlapped bands can be separated using the said isotopic exchange. The RNA H/D exchanges investigated in this work encompass three spatially distinct classes of base protons that exchange over greatly differing time regimes. The first class consists of imino (NH) and amino (NH_2) protons of the hydrogen-bond donating groups of the bases in single stranded RNA segments. The second class of exchangeable protons consists of the labile imino and amino protons of the bases that straddle the helical axis of double-stranded *A* RNA segments. For these double double-helical segments, the exchange of base imino and amino groups is presumed to require transient rupture and reformation of the Watson–Crick hydrogen bonds. In this breathing model, the hydrogen-bonded groups are available for exchange only during the transient open state. Accordingly, the hydrogen exchange rate is governed primarily by the lifetime of the open state [10]. The third type of exchangeable protons corresponds to the pseudoacidic 8CH groups of the RNA purines, which exchange relatively slowly [11]. Thus, the guanine and adenine 8CH/8CD exchange rates are an extraordinarily sensitive indicator of the local 7N–8C environments in the RNA minor groove, and their specific exchanges are retarded predictably by hydrogen bonding interactions of the purine 7N acceptor sites [12]. To facilitate the task of unravelling the information that remains hidden in broad bands consisting of many overlapping spectral features, two-dimensional (2D) correlation spectroscopy has been utilized [13]. We have used here 2D correlation spectroscopic analysis to resolve the dynamic molecular events that occur upon H/D exchange. H/D exchange of imino and amino protons and other exchangeable protons that have limited accessibility to their aqueous environment is dependent on the structural properties of RNA. The advantage of this study is that H/D exchange does not perturb the RNA secondary structure. The present study shows the potential of Raman, infrared and H/D exchange two-dimensional vibrational spectroscopy in probing the secondary and tertiary structure of RNA.

2. Experimental

2.1. Preparation of RNA

The complete 5′untranslated region of the HCV genome (nucleotides 1 to 341) was amplified by PCR from the plasmid pHCV-NC-Co which contains the HCV 5′untranslated and core coding regions. The sequence of the sense primer was 5′ **ATTTAAGGTGACACTATAG**GCCAGCCCCC-GATTGGGGG3′ and contained the sequence of the SP6 RNA polymerase promoter (shown in bold) and the sequence of the anti-sense primer was 5′GGTGCACGGTCTACGAGACC3′. After amplification, PCR products were purified using the GFX PCR DNA and Gel Band Purification kit (Amersham Biosciences, Buckinghamshire, UK) and in vitro transcribed using RiboMAX Large Scale RNA production System-SP6 kit (Promega Corporation, Madison WI) following the instruction supplied by the manufacturers. After synthesis, transcribed RNA was purified by phenol extraction followed by two rounds of isopropanol precipitation. The size and integrity of the RNA was checked by polyacrylamide gel electrophoresis and its concentration was determined by measuring the absorbance at 260 nm and using 25 g^{-1} cm^{-1} L as extinction coefficient.

2.2. Raman spectroscopy

The polynucleotide Raman spectra were measured in H_2O and D_2O solutions, pH 7.5, in 50 mM Tris buffer containing 0.1 M NaCl. Samples were placed in a quartz thermostated cuvette at 20 °C for Raman analysis. The spectral measurements were carried out on a Bruker RFS 100/S FT-Raman spectrometer with a Nd:YAG laser which emits at a wavelength of 1064 nm used as the excitation source. The scattered radiation was collected at 180° to the source, and typical spectra were recorded at 4 cm^{-1} resolution with 200 mW of laser power at the sample. Frequencies cited are accurate to ±0.5 cm^{-1}. Finally, 2000 scans were collected and averaged to yield spectra of suitable signal-to-noise ratio. Signals obtained were fed to a microcomputer for storage, display, plotting and processing, and the manipulation and evaluation of the spectra were carried out using the Grams/AI software (ThermoGalactic). This software was used to fit the 750–850 cm^{-1} region to a sum of Gaussians by a nonlinear least-squares procedure. The fit is in principle unique, which results from the restrictions that can be applied because some of the mathematical solutions do not agree with the theoretical basis, i.e., bands with negative heights, component band widths larger than the band width of the whole spectral profile to be fitted, etc. Linear baseline corrections were performed on the spectra in order to facilitate intensity comparisons. In all cases, the buffer was compensated by computer subtraction techniques. In this connection, the buffer spectra were always recorded with the same instrument settings employed for nucleic acid solutions.

2.3. Infrared spectroscopy

The infrared spectra were performed on a Perkin-Elmer 1725X Fourier transform IR spectrometer assisted by a personal computer. Spectra were measured under a resolution of 2 cm^{-1}. Special cells having either CaF_2 or ZnSe windows and 12 μm path length were used for measurement of the spectra. About 5 mg of RNA were dissolved in 100 μl of D_2O. During the first 5 min of the H/D exchange a spectrum was obtained every 60 s as an average of 8 scans. Subsequently, the measurement time interval was increased and the final spectrum was taken 4 h after the initiation of the exchange. To compensate for aqueous absorptions, the spectra of the nucleic acid-free solutions were also measured under the same experimental conditions as above in the same kind of cells. The instrument was continuously purged with dried nitrogen to remove water vapour, which was verified by a lack of features in the second derivative spectra of the 2000–1700 cm^{-1} absorption region.

2.4. Two-dimensional correlation analysis

We employed software named 2D-Pocha for the 2D correlation analysis written by Dr. Adachi and Dr. Y. Ozaki (Kwansei-Gakuin University, Japan). This 2D software was programmed on the basis of the developed algorithm of generalized two-dimensional correlation spectroscopy [13].

3. Results and discussion

3.1. Raman data

Fig. 1 shows the Raman spectra of 5′UTR of HCV RNA in H_2O and D_2O buffer. There is a region in these spectra that is of interest because of the conformational information which it contains, namely the 750–1600 cm^{-1} region. The Raman marker band near 815 cm^{-1} for C(3′)-endo-anti ribose conformation is plainly visible. This band is generated by a mode involving the ν_s(-OPO-) vibration (Table 1) and some stretching motion of ribofuranose ring bonds and seems to be consistent with the original assignments of the Raman marker bands for A-type nucleic acids [14,15]. Thus, it is well known that a medium-intensity band in the 820–800 cm^{-1} range is indicative of A-type conformation, while the shift of this band to the 840–820 cm^{-1} region is characteristic of the appearance of the B-type nucleic acid form. The conformational sensitivity of these nucleic acid backbone vibrations appears to arise from differences in the A- and B-type puckered furanose rings, which involve the C(3′)-endo-anti and C(2')-endo-anti conformations, respectively. A shoulder located near 830 cm^{-1} is also observed in the Raman spectrum of the 5′UTR sequence of HCV RNA (Table 1) which can be attributable to C(2′)-endo-anti conformations on the basis of the above spectrum–structure correlation. This means that, although the A-form secondary structure is found to be predominant in this polynucleotide, some nucleoside conformations can deviate from the C(3′)-endo ribofuranose pucker of the standard A-form in critical regions so that the polynucleotide chain folds into some complicated patterns of helices and loops. Thus, in addition to the C(3′)-endo ribofuranose form, C(2′)-endo sugar puckerings are also found which can be attributable to positions where chains are stretched and where chain foldings switch abruptly from helical to looped. In fact, this change in ribofuranose pucker has been reported to occur in the said structural motifs of tRNA [16]. In order to analyze these conformations in the 5′ UTR of HCV RNA, we examine in more detail the spectral profile in the 750–850 cm^{-1} region. Fig. 2 shows this region of the Raman spectrum of the 5′UTR in aqueous buffer. It is plotted on an expanded scale with the Raman spectrum resolved into a sum of Gaussian bands by the nonlinear least-squares program described above. The existence of two contributions near 805 and 815 cm^{-1} could be indicative of some difference

Table 1
Raman frequencies of 5′UTR of HCV RNA

H_2O solutions	D_2O solutions	Assignments
1691 sh	1691 sh	νC═O(2) (U)
1677 vs	1680 s	νC═O(4) (U), νC=O (G)
1644 m	1655 m	νC═O (G, C)
	1624 m	νC═C, νC═N (A, C, U)
1575 s	1579 vs	ν-ring (G, A)
1486 s	1481 s	ν-ring (G)
1423 m	1422 m	ν-ring (A), ribose
1377 m	1386 m	ν-ring (A, G)
1337 m	1341 m	ν-ring (A)
1305 m	1304 m	ν-ring (A)
1235 vs	1246 s	ν-ring (U)
1105 s	1105 s	$\nu_s PO_2^-$
923 w	923 w	ribose
877 w	–	ribose
830 sh	830 sh	ν_s(-OPO-)+ribose
816 m	813 m	ν_s(-OPO-)+ribose
784 vs	780 vs	ν-ring (U, C)
753 vw	753 vw	C
664 w	662 vw	G

Frequencies are accurate to ±2 cm^{-1} for strong bands and ±4 cm^{-1} for weak bands.
Abbreviations: A, adenine; U, uracil; G, guanine; C, cytosine; vs, very strong; s, strong; m, medium; w, weak; vw, very weak; sh, shoulder.

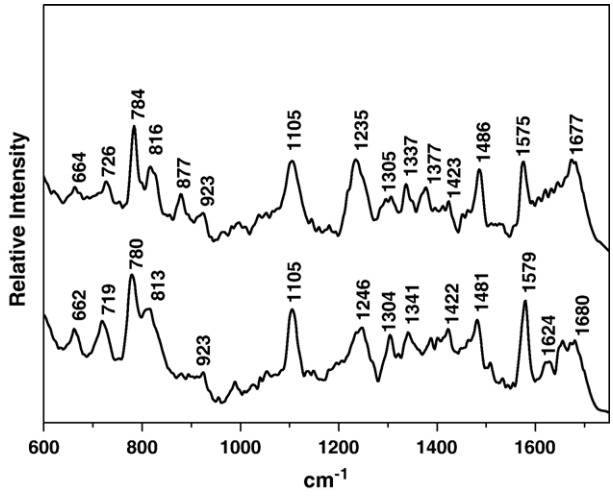

Fig. 1. Raman spectra of H_2O (upper) and D_2O (lower) solutions of 5′UTR RNA, pH 7.5, in 50 mM Tris buffer and 0.1 M NaCl.

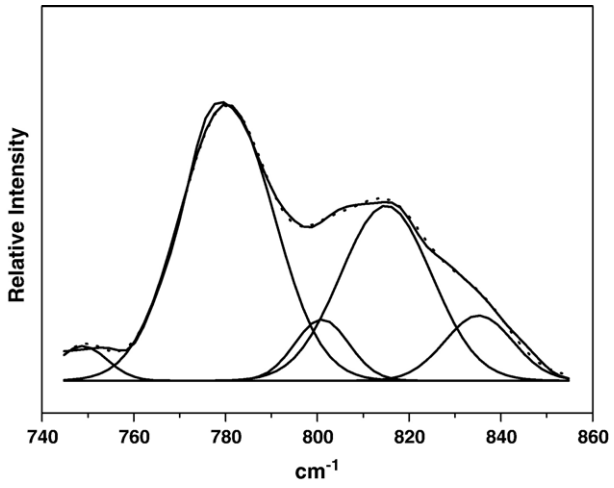

Fig. 2. Curve fitting of the Raman spectrum of 5′UTR RNA measured in D_2O solution, pD 7.5, in 50 mM Tris buffer and 0.1 M NaCl.

in the A-type geometry of the phosphodiester backbones of different chain segments. We clearly see also a band component near 830 cm^{-1} which is the canonical marker band for the C (2′)-endo ring pucker in RNA assigned to the sugar-phosphate backbone. The area percentage of this band component is found to be 19±1% (based on the sum of the 805, 815 and 830 cm^{-1} band areas), and interestingly this value is very near the proportion (18.7%) of nucleobases located at helix–loop junctions in a theoretical secondary structure model proposed on the basis of comparative sequence analysis and thermodynamic modelling [17]. Therefore, our spectroscopic results support the said secondary structural model and suggest that Raman spectroscopy can be used to determine the number of helical–looped junctions in RNA. Other Raman data are consistent with the above results. It is well known that bands in the 800–820 cm^{-1} range achieve intensity maxima in completely ordered structures, either double-stranded or single-stranded, and minima in completely disordered structures, irrespective of base composition or sequence in the polynucleotide in question [18]. We have used also these effects in order to know the percentage of RNA ribose-phosphate groups in ordered configurations of the 5′UTR molecule. The data required are the Raman intensities of the bands falling in the 800-840 and 1050–1120 cm^{-1} ranges attributable to ribose-phosphate backbone and $\nu_s PO_2^-$ motions, respectively. The $\nu_s PO_2^-$ band is considered to provide the best available basis for normalization of other Raman intensities of nucleic acids [18,19]. In solutions of polynucleotides, the intensity ratio (R) of the ribose-phosphate band around 815 cm^{-1} with respect to the $\nu_s PO_2^-$ one takes on values ranging from 0 to 1.64, depending upon the percentage of nucleotide residues which are present in segments of ordered secondary structure of the A type [20,21] including both the base-paired and base-stacked regions. Consequently, an R value of 1.11 obtained here is an indication that around 68±2% of the bases of 5′UTR are ordered (with C(3′)-endo ribofuranose pucker) under the conditions of our spectral measurements.

It is noteworthy that the $\nu_s PO_2^-$ band appears at 1105 cm^{-1}, which frequency is relatively high as compared with the position of this vibrational mode in B-DNA usually found near 1095 cm^{-1} [22]. This probably means that the O–H···O hydrogen bonding between water molecules and the PO_2^- oxygen is stronger in B than in the A-forms of 5′UTR.

In the nucleobase fingerprint region above 1150 cm^{-1}, measured in H_2O buffer (Table 1, Fig. 1), we observe a very strong band at 1235 cm^{-1} that can be assigned to base paired uracyls [23]. This intense band is accompanied by two shoulders at 1221 and 1248 cm^{-1} that can be attributable to unpaired uracyls and cytosines [24,25] on the basis of the positions of these bands for poly(rU) and poly(rC). Other base vibrations are observed at 1305 (adenine), 1337 (adenine), 1377 (both adenine and guanine), 1486 (guanine) and 1575 cm^{-1} (both adenine and guanine), among which the 1486 cm^{-1} one corresponds to a vibrational mode involving imidazole ring character [12,26]. Therefore this band has been found to be sensitive to the microenvironment at the 7N site of guanine imidazole ring [12,26] and can be applied to detect interactions involving 7N. The frequency of the 1486 cm^{-1} strong band is very near that of usual A-forms of RNA at 1485 cm^{-1} [12,18], and hence the shoulder located near 1475 cm^{-1} may correspond to free or base-paired guanine nucleobases interacting through 7N, as occurs for example in GGC triplets. The predominant bands in the 1600–1750 cm^{-1} region correspond to C═O, C═C and C═N stretching motions of free (unpaired) and paired nucleobases. On the basis of the Raman spectrum of single stranded poly(U) [27], the shoulder at 1691 cm^{-1} can be assigned to unpaired uracyls, which may be located in single stranded and/or looped regions.

3.2. Infrared data

In agreement with the Raman measurements, the infrared spectra confirm the coexistence of C(3′)-endo and C(2′)-endo sugar conformations through the phosphoester band at 814 cm^{-1} and the shoulder at 830 cm^{-1} respectively (Fig. 3A). In addition, the 863 cm^{-1} ribofuranose band and the antisymmetric $\nu_{as}PO_2^-$ one located at 1239 cm^{-1} reflect the RNA A form geometry which incorporates the C(3′)-endo nucleoside conformation [28]. The shoulder at 1225 cm^{-1} shows also a small proportion of C(2′)-endo ribofuranose pucker.

A particular structural feature of the RNA form in this 5′ UTR sequence is shown by deuteration of the RNA backbone described as follows. Fig. 3B shows the infrared spectra of 5′ UTR RNA and its deuterated derivative in the 1200–950 cm^{-1} region. An information concerning the structure-promoting effect of the 2′OH is given by frequency shifting that is generated by coupling of the ν_sCOC ether vibration of the ribose residues and the bending motion of the 2′OD group in the 1100–1000 cm^{-1} range. Band shifting in opposite directions upon deuteration as a result of coupling between vibrations (Fermi resonance) is thus observed, caused by a mechanical interaction of vibrational transitions [29]. This mechanical coupling involves the anharmonic terms of the potential and is induced directly through the electron system by a contact of the neighbouring groups with the coupling vibrations via intermolecular bonding, for instance a hydrogen bond [30]. In the

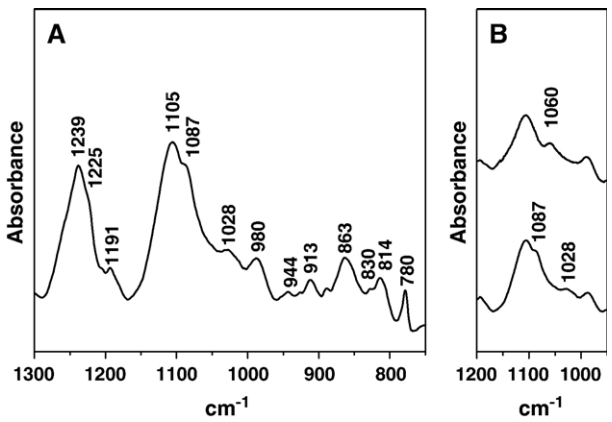

Fig. 3. Infrared spectra of aqueous solutions of 5′UTR RNA, pH 7.5, in 50 mM Tris buffer and 0.1 M NaCl: (A) in D_2O buffer; (B) in H_2O (upper) and D_2O (lower) buffers.

non-deuterated 5′UTR RNA, the vibration of the ether group of the ribose residue appears at 1060 cm^{-1}. On H/D exchange the δ2′OD vibration is observed at 1028 cm^{-1}. Further one can see that the 1060 cm^{-1} ether vibration is shifted, on coupling with the δ2′OD vibration, towards higher frequencies and merges into the absorption band located at 1087 cm^{-1}. The fact that the ν_sCOC ether vibration and the δ2′OD vibration couple proves that the 2′OH group is linked with the neighbouring ribose residue via hydrogen bonding, which has been found to occur also in double helical regions of 23 S RNA and $tRNA^{Phe}$ [31].

The gradual H/D isotopic exchange allows for the study of exchangeable protons in 5′UTR of viral RNA. The bands appearing in the 1800–1500 cm^{-1} range can be effectively used to monitor RNA structural changes that involve alteration of base stacking, base pairing and ligand binding to specific nucleobases. These bands mainly originate from double bond stretching vibrations such as νC═O, νC═N and νC═C. The H/D exchange of the labile NH_2 and NH groups cause frequency downshifting to positions out of this region. The bending motions of the NH_2 and NH groups are coupled to the above double bond stretching vibrations, hence a decreasing intensity or narrowing of the spectral profile in the 1700–1600 cm^{-1} region is observed upon deuteration of the 5′UTR RNA (Fig. 4). One of the goals of our infrared measurements is enhancing spectral resolution and determining the order of events during isotopic H/D exchange by use of two-dimensional (2D) correlation analysis. The synchronous correlation plot (Fig. 5A) displays auto peaks on the diagonal reflecting those spectral signals that are perturbed as a function of time by H/D exchange. Cross peaks (placed off-diagonally) are observed for bands that exhibit (at least partially) correlated dynamic behaviour. Cross peaks, which can either be positive or negative, reflect correlated changes of functional groups within the RNA that occur simultaneously in the same (+) or in the opposite (−) direction. By contrast, the asynchronous 2D correlation plot (Fig. 5B) is characterized by missing auto peaks and asymmetric cross peaks which reveal uncorrelated (i.e., out-of-phase) behaviour of two bands. Auto peak positions determined from the synchronous plot (Fig. 5A) are summarized in Table 2. Assignments of these peaks to either single stranded (ss) or double stranded (ds) nucleobases are as follows: ds-uracil (1700 cm^{-1}); ss-uracil and ss-G (1693 cm^{-1}); ss-

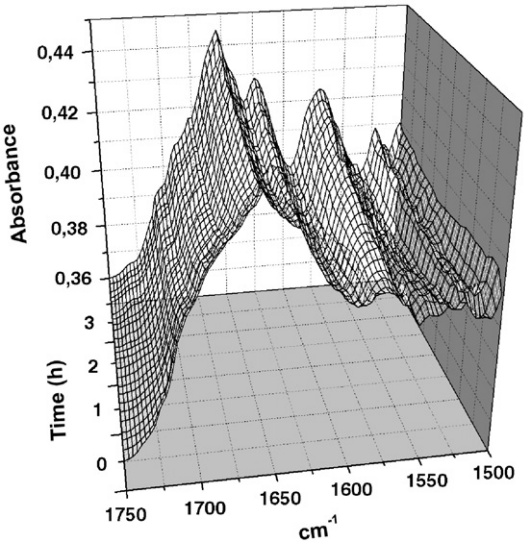

Fig. 4. Infrared spectra of 5′UTR RNA during the course of H/D exchange. Data were collected from H_2O solutions at pH 7.5 in 50 mM Tris buffer and 0.1 M NaCl.

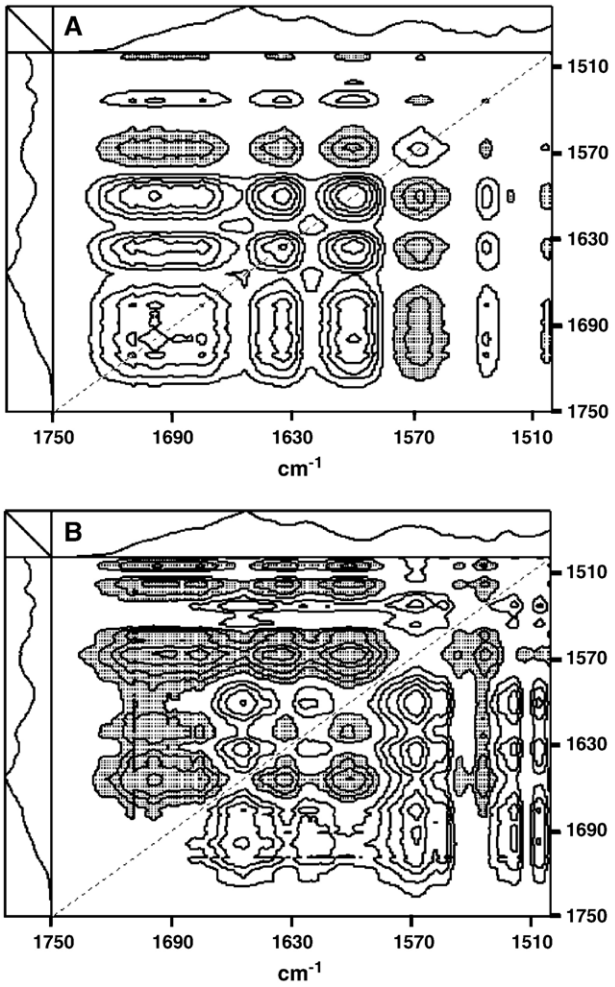

Fig. 5. (A) Synchronous and (B) asynchronous 2D IR correlation plots of 5′ UTR RNA calculated from the spectra measured in the course of H/D exchange.

Table 2
Auto peak positions of the synchronous plot from H/D exchange in the 1750–1500 cm^{-1} infrared region of the 5′UTR of HCV RNA

Synchronous	Assignment
1700	ds-U
1693	ss-U, ss-G
1676	ss-G, ds-U
1656	ss-A, ss/ds-C
1635	ss-G, ss-U, ds-A
1620	ss-A, ss/ds-C
1600	ss-G, ss-A, ss-C
1565	ss/ds-G
1533	ds-C, ss/ds-G

Abbreviations: ss, single-stranded; ds, double-stranded; A, adenine; U, uracil; G, guanine; C, cytosine.

Table 3
Asynchronous plot analysis used to determine H/D exchange dynamics in the HCV 5′UTR

Cross peak (cm^{-1})	H/D exchange dynamics
(1655, 1698)	ss-A, ss-C (1655 cm^{-1}) prior to ds-U (1698 cm^{-1})
(1633, 1655) (opp)	ss-A, ss-C (1655 cm^{-1}) prior to ss-G, ds-A (1633 cm^{-1})
(1620, 1698)	ss-A, ss-C (1620 cm^{-1}) prior to ds-U (1698 cm^{-1})
(1620, 1676)	ss-A, ss-C (1620 cm^{-1}) prior to ss-G (1676 cm^{-1})
(1620, 1633)	ss-A, ss-C (1620 cm^{-1}) prior to ds-A, ss-G (1633 cm^{-1})
(1602, 1655) (opp)	ss-A, ss-C (1655 cm^{-1}) prior to ss-G (1602 cm^{-1})
(1602, 1620) (opp)	ss-A, ss-C (1620 cm^{-1}) prior to ss-G (1602 cm^{-1})
(1568, 1693) (opp)	ss-U (1693 cm^{-1}) prior to ds/ss-G (1568 cm^{-1})
(1568, 1676) (opp)	ss-G, ds-U (1676 cm^{-1}) prior to ds-G (1568 cm^{-1})
(1568, 1633) (opp)	ss-U, ds-A, ss-G (1633 cm^{-1}) prior to ds-G (1568 cm^{-1})
(1568, 1602) (opp)	ss-A, ss-C (1602 cm^{-1}) prior to ds/ss-G (1568 cm^{-1})
(1533, 1655) (opp)	ss-A, ss-C (1655 cm^{-1}) prior to ds-C, ds/ss-G (1533 cm^{-1})
(1533, 1568) (opp)	ss-G (1568 cm^{-1}) prior to ds-C, ds-G (1533 cm^{-1})
(1519, 1693)	ss-C (1519 cm^{-1}) prior to ss-G (1993 cm^{-1})
(1519, 1676)	ss-C (1519 cm^{-1}) prior to ds-U, ss-G (1676 cm^{-1})
(1519, 1633)	ss-C (1519 cm^{-1}) prior to ds-A, ss-G (1633 cm^{-1})
(1519, 1601)	ss-C (1519 cm^{-1}) prior to ss-G (1601 cm^{-1})

Abbreviations: opp, opposite signs of the synchronous and asynchronous cross peaks; ss, single-stranded; ds, double-stranded; A, adenine; U, uracil; G, guanine; C, cytosine.

guanine and ds-uracil (1676 cm^{-1}); ss/ds-cytosine and ss-adenine (1656 cm^{-1}); ss-uracil, ss-guanine and ds-adenine (1635 cm^{-1}); ss-adenine and ss/ds cytosine (1620 cm^{-1}); ss-adenine, ss-cytosine and ss-guanine (1600 cm^{-1}); ss/ds-guanine (1565 cm^{-1}); ds-cytosine and ss/ds-guanine (1533 cm^{-1}) [8,32–35]. Correlation peaks determined from the asynchronous plot (Fig. 5B) and the plot analysis of the H/D exchange dynamics in the 5′UTR polynucleotide are summarized in Table 3. The asynchronous plot (Fig. 5B) provides a clear picture of the order of the events upon isotopic perturbation of the RNA sample. Thus, cross peaks with the same sign in the synchronous and asynchronous plots indicate that a spectral change of the ν_1 (abscissa) band occurs predominantly before that of the ν_2 (ordinate) band in the sequential order of time. For opposite signs of the synchronous and asynchronous cross peaks, the temporal order is reversed [13]. On this basis, although the asynchronous cross peaks at (1568, 1602 cm^{-1}), (1568, 1633 cm^{-1}), (1568, 1676 cm^{-1}) and (1568, 1693 cm^{-1}) have positive sign, the intensity change of the 1568 cm^{-1} band (ds-guanine) occurs after the changes located at 1602 cm^{-1}, 1633 cm^{-1}, 1676 cm^{-1} (ss-guanine, ds-uracil) and 1693 cm^{-1} (ss-uracil, ss-guanine) [28] because of the synchronous correlation intensity at the above cross peaks is negative ($\Phi(\nu_1, \nu_2)<0$). As the 1568 cm^{-1} band can be assigned to double stranded guanine residues [8], the triple hydrogen bonded guanine is deuterated after the A·U base pairs and single stranded adenine, uracil, guanine and cytosine nucleobases. On the basis of the above assignment, the negative cross peak at (1600, 1620 cm^{-1}) can be interpreted in the sense that there are single stranded cytosine, guanine and adenine nucleobases in the 5′UTR viral RNA where deuteration is slower for the guanine ones probably due to the four hydrogen bonding sites of this purine base. The cross peak at (1655, 1698 cm^{-1}) suggests that the exchange of A·U base pairs is slower than those of single stranded adenine and cytosine. The absence of this cross peak in the synchronous plot involves that the intensities at 1655 and 1698 cm^{-1} vary mainly through uncorrelated (i.e., out-of-phase) way. Moreover, the exchange dynamics shown by the (1655, 1698 cm^{-1}) cross peak is consistent with that located at (1620, 1633 cm^{-1}) (Table 3). On the basis of the above results, we can state that roughly three kinetics classes of exchanging nucleobases can be considered for the 5′UTR RNA of HCV virus, namely, G·C base pairs, A·U base pairs and single stranded A, U, G and C, and the H/D exchange dynamics of these nucleobases depends mainly on their single or double stranded state. In some cases, however, some synchronous cross peaks correlating ds-base bands and ss-base bands can be observed, as occurs for that located at (1600, 1700 cm^{-1}) (Fig. 5A). This peak can be assigned to double stranded A·U bases which are synchronously deuterated with some single stranded (non Watson–Crick base paired) adenine bases. This interpretation is consistent with the presence of some A*A·U triplets, which seem to be also present in the junction of two isolated helical segments of the 5′UTR RNA [7]. As the temperature for dissociation of the third adenine base in these triplets is very close to that for dissociation of the corresponding Watson–Crick A·U base pair [36], it is not surprising that the deuteration of the A·U base pair in the above A*A·U triplets occurs synchronously with the deuteration of the third adenine base. In this connection, synchronous two-dimensional correlation maps obtained through FTIR-monitoring of H/D exchange can be useful to identify nucleobase triplets in relation to the tertiary structure of RNA.

In conclusion, we have shown here that Raman spectroscopy, by its capability to elucidate local nucleoside conformations, permits the analysis of helix–loop junctions in the 5′UTR RNA of HCV virus. We have found that the percentage of nucleobases involved in these junctions is very close to that of a theoretical secondary structure model proposed previously using comparative sequence analysis and thermodynamic modelling [17], and around 68% of the nucleobases of this polynucleotide are ordered under the conditions of our spectral measurements. In order to get insights into the tertiary structure of this polynucleotide, we have FTIR-monitored the temporal events that occur during the H/D exchange perturbation. Guanine and cytosine nucleobases involved in base-pair secondary structure retard the rate of isotopic exchange. A likely source of such restricted exchange is the hydrogen bonding strength in GC base pairs. On the other hand, part of the infrared intensity change of A·U base pairs at 1700 cm^{-1} can be synchronously correlated with intensity change of adenine at 1600 cm^{-1}, which is consistent with the presence of junction A*A·U triplets in the 5′UTR RNA. H/D exchange reveals also that the 2′OH ribose groups are cross-linked with the oxygen ether atoms of the neighbouring ribose residues via hydrogen bonds. Further experiments designed to determine the effects of encapsidation on the structure of this RNA are in progress.

Acknowledgements

We thank the Spanish Ministerio de Educación y Ciencia for financial support (Project BQU2003-01690). Arantxa Rodriguez-Casado expresses her gratitude to CSIC for her I3P grant (European Social Fund).

References

[1] F. Penin, J. Dubuisson, F.A. Rey, D. Moradpour, J.M. Pawlotsky, Structural biology of hepatitis C virus, Hepatology 39 (2004) 5--19.
[2] P. Simmonds, E.C. Holmes, T.A. Cha, S.W. Chan, F. McOmish, B. Irvine, E. Beall, P.L. Yap, J. Kolberg, M.S. Urdea, Classification of hepatitis C virus into six major genotypes and a series of subtypes by phylogenetic analysis of the NS5 region, J. Gen. Virol. 74 (1993) 2391--2399.
[3] S. Bhattacharyya, K. Mapa, S. Prabhavathi, S.R. Sudhamani, P.K. Menon, K.P.J. John, C. Shivaram, S. Amarnath, S. Das, Phylogenetic conservation of the stem–loop III structure of the 5′untranslated region of hepatitis C virus RNA among natural variants in samples collected from southern India, Arch. Virol. 149 (2004) 1015--1026.
[4] J. Hall, D. Hüsken, R. Häner, Towards artificial ribonucleases: the sequence-specific cleavage of RNA in a duplex, Nucleic Acids Res. 24 (1996) 3522--3536.
[5] D. Hüsken, G. Goodball, M.J. Blommers, W. Jahnke, J. Hall, R. Häner, H. E. Moser, Creating RNA bulges: cleavage of RNA in RNA/DNA duplexes by metal ion catalysis, Biochemistry 35 (1996) 16591--16600.
[6] S. Portmann, S. Grimm, C. Workman, N. Usman, M. Egli, Crystal structures of an A-form duplex with single-adenosine bulges and a conformational basis for site-specific RNA self-cleavage, Chem. Biol. 3 (1996) 173--184.
[7] J.S. Kieft, K. Zhou, A. Grech, R. Jubin, J.A. Doudna, Crystal structure of an RNA tertiary domain essential to HCV IRES-mediated translation initiation, Nat. Struct. Biol. 9 (2002) 370--374.
[8] M. Banyay, M. Sarkar, A. Gräslund, A library of IR bands of nucleic acids in solution, Biophys. Chemist. 104 (2003) 477--488.
[9] R. Tuma, G.J. Thomas Jr., Raman spectroscopy of viruses, in: J.M. Chalmers, P.R. Griffiths (Eds.), Handbook of Vibrational Spectroscopy, John Wiley and Sons, Chichester, 2002, pp. 1--17.
[10] S.W. Englander, N.R. Kallenbach, Hydrogen exchange and structural dynamics of proteins and nucleic acids, Q. Rev. Biophys. 4 (1984) 521--655.
[11] K.E. Reilly, G.J. Thomas Jr., Hydrogen exchange dynamics of the P22 virion determined by time-resolved Raman spectroscopy, J. Mol. Biol. 241 (1994) 68--82.
[12] J.M. Benevides, G.J. Thomas Jr., Dependence of purine 8C–H exchange on nucleic acid conformation and base-pairing geometry. A dynamic probe of DNA and RNA secondary structures, Biopolymers 24 (1985) 667--682.
[13] I. Noda, Y. Ozaki, Two-Dimensional Correlation Spectroscopy. Applications in Vibrational and Optical Spectroscopy, John Wiley and Sons, Chichester, England, 2004.
[14] K.C. Lu, E.W. Prohofsky, L.L. Van Zandt, Vibrational modes of A-DNA, B-DNA and A-RNA backbones: an application of a green-function refinement procedure, Biopolymers 16 (1977) 2491--2506.
[15] G.A. Thomas, W.L. Peticolas, Flexibility of nucleic acid conformations: 1. Comparison of the intensities of the Raman-active backbone vibrations in double-helical nucleic acids and model double-helical dinucleotide crystals, J. Am. Chem. Soc. 105 (1983) 986--992.
[16] W. Saenger, Principles of Nucleic Acid Structure, Springer-Verlag, New York, 1984.
[17] E.A. Brown, H.C. Zhang, L.H. Ping, S.M. Lemon, Secondary structure of the 5′-nontranslated regions of hepatitis-C virus and pestivirus genomic RNAs, Nucleic Acids Res. 20 (1992) 5041--5045.
[18] M.C. Chen, R. Giegé, R.C. Lord, A. Rich, Raman spectra of ten aqueous transfer RNAs and 5S RNA, conformational comparison with yeast phenylalanine transfer RNA, Biochemistry 17 (1978) 3134--3138.
[19] J.M. Benevides, G.J. Thomas Jr., A solution structure for poly(rA)(poly (dT) with different furanose pucker and backbone geometry in rA and dT strands and intrastrand hydrogen bonding of adenine 8CH, Biochemistry 27 (1988) 3868--3873.
[20] G.J. Thomas Jr., M.C. Chen, K.A. Hartman, Raman studies of nucleic acids X. Conformational structures of *Escherichia coli* transfer RNAs in aqueous solution, Biochim. Biophys. Acta 324 (1973) 37--49.
[21] G.J. Thomas Jr., B. Prescott, M.G. Hamilton, Raman spectra and conformational properties of ribosomes during various stages of disassembly, Biochemistry 19 (1980) 3604--3613.
[22] B. Prescott, W. Steinmetz, G.J. Thomas Jr., Characterization of DNA structures by laser Raman spectroscopy, Biopolymers 23 (1984) 235--256.
[23] L. Lafleur, J. Rice, G.J. Thomas Jr., Raman studies of nucleic acids. VII. PolyA (polyU and polyG·polyC, Biopolymers 11 (1972) 2423--2437.
[24] C.H. Chou, G.J. Thomas Jr., Raman spectral studies of nucleic acids. XVI. Structures of polyribocytidylic acid in aqueous solution, Biopolymers 16 (1977) 765--789.
[25] J. Liquier, C. Gouyette, T. Huynh-Dinh, E. Taillandier, Spectroscopic studies of chimeric DNA–RNA and RNA 29-base intramolecular triple helices, J. Raman Spectrosc. 30 (1999) 657--666.
[26] P. Carmona, P.V. Huong, E. Gredilla, Raman spectra and binding of Cu^{II} to purine nucleotides, J. Raman Spectrosc. 19 (1988) 315--319.
[27] T. O'Connor, M. Bina, The structure of triple helical poly(U)(poly(A)(poly (U) studied by Raman spectroscopy, J. Biomol. Struct. Dyn. 2 (1984) 615--625.
[28] J. Liquier, E. Taillandier, R. Klinck, E. Guittet, C. Gouyette, T. Huynh-Dinh, Spectroscopic studies of chimeric DNA–RNA and RNA 29-base intramolecular triple helices, Nucleic Acids Res. 23 (1995) 1722--1728.
[29] N.L. Alpert, W.E. Keiser, H.A. Szymanski, Theory and Practice of IR Spectroscopy, Plenum, New York, 1970.
[30] P. Carmona, M. Molina, N. Aboitiz, C. Vicent, Vibrational coupling as diagnostic for intramolecular hydrogen bonds in carbohydrates in aqueous solution, Biopolymers 67 (2002) 20--25.
[31] R. Herbeck, G. Zundel, Influence of temperature and magnesium ions on the secondary and tertiary structures of tRNAPhe and 23 S RNA. Infrared investigations, Biochim. Biophys. Acta 418 (1976) 52--62.
[32] H.T. Miles, J. Frazier, Infrared spectroscopy of polynucleotides in the carbonyl region in H_2O solution: a·U systems, Biochemistry 17 (1978) 2920--2927.
[33] P. Carmona, M. Molina, A. Lasagabaster, R. Escobar, Determination of the hydrogen-bonded structure of CGG trimers in chloroform solution by vibrational spectroscopy, Biospectroscopy 1 (1995) 235--245.
[34] M. Sarkar, U. Dornberger, E. Rozners, H. Fritzsche, R. Strömberg, A. Gräslund, FTIR spectroscopic studies of oligonucleotides that model a triple-helical domain in self-splicing group I introns, Biochemistry 36 (1997) 15463--15471.
[35] A.G. Petrovic, P.L. Polavarapu, Structural transitions of polyriboadenylic acid induced by the changes in pH and temperature: vibrational circular dichroism study in solution and film states, J. Phys. Chem., B 109 (2005) 23698--23705.
[36] C. Dagneaux, H. Gousset, A.K. Shchyolkina, M. Ouali, R. Letellier, J. Liquier, V.L. Florentiev, E. Taillandier, Parallel and antiparallel A∗A–T intramolecular triple helices, Nucleic Acids Res. 24 (1996) 4506--4512.